

THE DISCOVERY OF A LARGE Ly α +He II NEBULA AT $z \approx 1.67$: A CANDIDATE LOW METALLICITY REGION?

MOIRE K. M. PRESCOTT¹, ARJUN DEY², AND BUELL T. JANNUZI²

Draft version June 29, 2009

ABSTRACT

We have discovered a ≈ 45 kpc Ly α nebula (or Ly α “blob”) at $z \approx 1.67$ which exhibits strong, spatially-extended He II emission and very weak C IV and C III] emission. This is the first spatially-extended Ly α +He II emitter observed and the lowest redshift Ly α blob yet found. Strong Ly α and He II $\lambda 1640$ emission in the absence of metal lines has been proposed as a unique observational signature of primordial galaxy formation (e.g., from gravitational cooling radiation or Population III star formation), but no convincing examples of spatially-extended Ly α +He II emitters have surfaced either in Ly α -emitting galaxy surveys at high redshifts ($z > 4$) or in studies of Ly α nebulae at lower redshifts. From comparisons with photoionization models, we find that the observed line ratios in this nebula are consistent with low metallicity gas ($Z \lesssim 10^{-2} - 10^{-3} Z_{\odot}$), but that this conclusion depends on the unknown ionization parameter of the system. The large He II equivalent width ($\approx 37 \pm 10 \text{ \AA}$) and the large He II/Ly α ratio (0.12 ± 0.04) suggest that the cloud is being illuminated by a hard ionizing continuum, either an AGN or very low metallicity stars, or perhaps powered by gravitational cooling radiation. Thus far there is no obvious sign of a powerful AGN in or near the system, so in order to power the nebula while remaining hidden from view even in the mid-infrared, the AGN would need to be heavily obscured. Despite the strong Ly α +He II emission, it is not yet clear what is the dominant power source for this nebula. The system therefore serves as an instructive example of how the complexities of true astrophysical sources will complicate matters when attempting to use a strong Ly α +He II signature as a unique tracer of primordial galaxy formation.

Subject headings: galaxies: formation — galaxies: high-redshift — galaxies: surveys

1. INTRODUCTION

Understanding primordial galaxy formation is a major science driver for the next generation of large space- and ground-based telescopes and has inspired a substantial amount of theoretical literature due to the potential contribution of the first generations of stars to reionization and the early stages of galaxy evolution. According to theoretical predictions, the observational signature of primordial galaxy formation is the presence of strong Ly α $\lambda 1216$ and He II $\lambda 1640$ emission lines, either due to photoionization by very low metallicity and Population III (Pop III, i.e., zero metallicity) star formation (e.g., Tumlinson et al. 2001; Schaerer 2003, 2008) or due to gas cooling during gravitational collapse (e.g., Haiman et al. 2000; Yang et al. 2006). In the case of Pop III stars, the strong Ly α and He II is a direct consequence of the low metallicities, where, in the absence of metals, H and He become the dominant line coolants for the gas, and of the hot effective temperatures of Pop III stellar clusters, which are predicted to show a top-heavy IMF and low stellar atmospheric opacity due to the lack of metals (e.g., Ezer & Cameron 1971; Bromm et al. 2001). In the case of gravitational cooling radiation, Ly α and He II are the primary ways for pristine gas to cool as it is collisionally excited during gravitational collapse; the predicted He II/Ly α ratios may be as high as 10% (e.g., Haiman et al. 2000; Yang et al. 2006). Strong Ly α and He II emission lines are commonly seen in other as-

trophysical sources with hard ionizing continua, but at normal metallicities they are generally accompanied by strong metal lines such as C III] and C IV, as seen for example, in AGN, radio galaxy halos, Wolf-Rayet galaxies, or cases of shock ionization (e.g., Reuland et al. 2007; Leitherer et al. 1996; Dopita & Sutherland 1996). The presence of strong Ly α and He II emission in the absence of strong metal lines has been put forward as a potentially unique observational signature of primordial galaxy formation.

Although theoretical studies suggest that Pop III and very low metallicity star formation may persist down to lower redshifts, this depends on the feedback efficiency, i.e., the ability of a Pop III stellar population to pollute the large-scale surroundings with metals (e.g., Tornatore et al. 2007). Searches for Pop III stars have understandably pushed to higher redshift ($z > 4$), where the Pop III star formation rate density should increase dramatically relative to that found in the local Universe (Scannapieco et al. 2003). Thus far, no unambiguous case of a Pop III stellar population has been observed. Several Ly α -emitting galaxy studies at $z \sim 4 - 5$ have uncovered sources with unusually high Ly α equivalent widths ($W_{rest} > 240 \text{ \AA}$) – larger than that expected from a normal stellar population – suggesting either a top-heavy IMF, a very low metallicity, and/or a very young age (Malhotra & Rhoads 2002; Rhoads et al. 2003). However, the complicated radiative transfer of Ly α in a clumpy ISM could also be responsible for boosting the Ly α (Finkelstein et al. 2008), and in these studies, no corroborating evidence for the Pop III scenario in the form of a strong He II detection was found in either the individual or stacked LAE spectra, leaving the mat-

¹ Steward Observatory, University of Arizona, Tucson, AZ 85721; mprescott@as.arizona.edu

² National Optical Astronomy Observatory, 950 North Cherry Avenue, Tucson, AZ 85719; dey@noao.edu, jannuzi@noao.edu

ter unresolved (Dawson et al. 2004; Ouchi et al. 2008). Deep spectroscopic observations of a strong Ly α -emitting galaxy at $z \approx 6.33$ showed no evidence for He II emission (Nagao et al. 2005), and a more recent Ly α +He II dual emitter survey at $z \sim 4 - 5$ found no convincing candidates (Nagao et al. 2008). The limits from each of these studies suggest that Pop III star formation does not dominate in these $z \sim 4 - 5$ samples, prompting the authors to encourage searches at ever higher redshifts ($z \gtrsim 7$). Additional high redshift Ly α +He II surveys are underway (e.g., di Serego Alighieri et al. 2008).

In this paper we report on the discovery of a $z \approx 1.67$ Ly α nebula with strong, spatially-extended He II emission and very weak C IV and C III] emission. This is the first spatially-extended source that resembles the predicted Ly α +He II signature of primordial galaxy formation. However, the system is more complex than it first appears. The observed line ratios suggest that the nebula may contain low metallicity gas, but this depends on the unknown ionization parameter of the system. Detailed analysis of the spectra along with extensive multi-wavelength data reveals that the source of ionization is uncertain: the nebula is either an H II region ionized by a hard spectrum source, i.e., an AGN or a very low metallicity stellar population, or a gravitationally cooling cloud. The fact that multiwavelength follow-up observations are required in order to better constrain the source(s) of ionization and metallicity of the nebula has implications for Ly α +He II searches at higher redshift. In Section 2, we summarize the systematic search for Ly α nebulae that led to this discovery and our observations and reductions. Section 3 contains a discussion of the observational results, and Section 4 details our analysis of the physical properties of the nebula. In Section 5 we discuss the implications of this discovery for the ongoing high redshift Ly α +He II surveys, and we summarize our conclusions in Section 6.

We assume the standard Λ CDM cosmology ($\Omega_M=0.3$, $\Omega_\Lambda=0.7$, $h=0.7$); 1'' corresponds to a physical scale of 8.47 kpc at $z = 1.671$. All magnitudes are in the AB system. Unless otherwise stated, He II refers to He II λ 1640Å, C IV to C IV λ 1549,1550, C III] to C III] λ 1909, and Ne IV] to Ne IV] λ 2424.

2. OBSERVATIONS & REDUCTIONS

In this section we discuss the observations that led to the discovery of this Ly α +He II nebula and the methods used to process the imaging and spectroscopic data.

2.1. The Search

Large Ly α nebulae (or Ly α “blobs”) – large (~ 100 kpc) clouds of gas emitting strongly in Ly α – are thought to be sites of ongoing galaxy formation and have been found in small numbers, primarily at $2 < z < 3$. Early theoretical work suggested that these nebulae could be examples of gravitationally cooling clouds (Haiman et al. 2000), and more recent cosmological hydrodynamic simulations indicated that cooling clouds should be detectable as Ly α +He II nebulae, although the specific predictions proved uncertain due to the treatment of star-forming gas (Yang et al. 2006; Y. Yang 2008, private communication). Several of the largest Ly α nebulae, including one with strong He II and C IV emission (Dey et al. 2005), have since been shown

to be powered instead by AGN, spatially-extended star formation, or some combination (e.g., Dey et al. 2005; Matsuda et al. 2007; Geach et al. 2007). Two groups claim to have discovered Ly α nebulae that are powered by gravitational cooling radiation (Nilsson et al. 2006; Smith & Jarvis 2007; Smith et al. 2008), but neither case shows strong He II emission.

Ly α nebulae are extremely rare objects and have often been found using deep narrow-band imaging surveys of known galaxy overdensities. As such, their space density, particularly at the bright end of the luminosity function, is largely unconstrained. In order to carry out an efficient but unbiased survey of a large cosmic volume, we have designed a systematic morphological search for spatially-extended Ly α nebulae using the *broad-band* imaging from the NOAO Deep Wide-Field Survey (NDWFS; Jannuzi & Dey 1999) Boötes Field. This field has been imaged in B_W , R , and I -band with median 5σ point-source depths of ≈ 27.1 , 26.3, and 25.8 mag (AB), respectively. In the sub-field relevant to this paper, the B_W , R , and I -band 5σ point-source depths are 27.5, 26.1, and 26.0 mag for 2.3, 1.7, and 2.8 hrs of integration, respectively. Candidates were selected from the broad-band data using a morphological and color selection algorithm, and spectroscopic follow-up was used to rule out low-redshift interlopers. The advantage of using broad-band data to search for line-emitting sources, a seemingly crude approach, is the enormous comoving volumes ($\sim 10^8 h_{70}^{-3} \text{ Mpc}^3$) that can be surveyed efficiently using publicly available data over wide fields. The success of the present survey relied heavily on the depth of the broad-band NDWFS imaging and the darkness of the sky within the B_W -band, against which strong line emission can dominate the flux even within the very broad B_W filter.

A full discussion of the search algorithm and results will be discussed elsewhere (Prescott et al. 2009, in preparation). Here we report on the discovery of a new Ly α +He II nebula at $z \approx 1.67$ (hereafter denoted PRG1) located in the Boötes field at 14:35:12.439 +35:11:07.16 (J2000). Unlike the other Ly α sources found in our systematic search, the Ly α +He II nebula presented here was selected by the search algorithm not because of its Ly α emission, which lies outside the B_W filter, but instead because of the strong and diffuse blue continuum emission ($\approx 92\%$) and spatially-extended He II emission ($\approx 8\%$) within the bandpass. Postage stamps from GALEX (FUV & NUV; Martin et al. 2005), the NOAO Deep Wide-Field Survey (B_W , R , and I), and the Spitzer Deep Wide-Field Survey (SDWFS; IRAC 3.6 μ m, 4.5 μ m, 5.8 μ m, and 8.0 μ m; Ashby et al. 2009, submitted) are shown in Figure 1. The GALEX limits are 0.36 μ Jy in the NUV and FUV bands; the SDWFS limits are 3.2, 4.4, 25.5, and 25 μ Jy (5σ). The MIPS coverage of this region shows no detection with a 1σ rms limit of 51 μ Jy (E. Le Floch 2008, private communication).

2.2. Spectroscopic Follow-up

We obtained spectroscopic follow-up observations using the MMT and the Blue Channel Spectrograph during UT 2008 June 8-9 as part of our systematic search for Ly α nebulae. We used a $1.5 \times 120''$ (unvignetted) slit and the 300 l/mm grating ($\lambda_c \approx 5713\text{Å}$, $\Delta\lambda \approx 3100 - 8320\text{Å}$). We chose a slit orientation that spanned the longest

dimension of the diffuse emission (PA=81.2°, observed near transit), as shown in Figure 1, while also intersecting a nearby bright object. We moved the target along the slit by $\approx 5''$ inbetween exposures.

Conditions during the first night were clear and stable with 1'' seeing; the second night was clear but with variable seeing ($\gtrsim 1.3''$) and high winds which caused shaking of the telescope pointing. We show in Section 3.2 that due to a slight pointing offset and wind-shake the data from the second night sample a different spatial region within the nebula and are contaminated at some level by sources nominally off the slit, in particular a red compact source to the WNW (Source A in Figure 1). For this reason, data from the two nights were reduced and analyzed separately. The most robust Ly α and He II flux measurements are from the first night, when conditions were excellent during the single half hour exposure. An additional 1.5 hours of integration were obtained during the second night. The Ly α flux measurement from Night 2 shows a 25% loss relative to that from Night 1. In the remainder of the paper we use the Ly α and He II flux measurements from Night 1 but include the line ratios derived from both nights.

The data were reduced using IRAF³. After performing the overscan and bias subtraction, we corrected flatfield exposures for the response of the internal ‘Bright Continuum’ flatfield lamp by dividing out the median along columns and then applied the flatfield correction. We used twilight flats to determine the illumination correction for the science frames. Cosmic rays were removed using *xzap*⁴. The wavelength solution was determined using HeArNe and HgCd comparison lamps, with an rms of $\approx 0.17\text{\AA}$. We corrected the data for a slight systematic offset in the night sky lines; the night sky line wavelengths in the final spectra are correct to $\pm 0.3\text{\AA}$. Flux calibration was based on observations of the standard stars BD+33 2642 and Wolf 1346⁵. We applied a grey shift ($\lesssim 0.08$ mag) and fit the sensitivity function using extra care at the blue end of the spectrum because the Ly α line at $\approx 3250\text{\AA}$ lies only 56.3 pixels (109.7 \AA) from the edge of the chip. The instrumental resolution measured from the Hg I λ 4047 line is 3.6 \AA , and the tilt within the aperture is $\leq \pm 5.24 \text{ km s}^{-1}$ over the region of the nebula.

3. RESULTS

3.1. Ly α and He II Emission

The final 2D and 1D spectra from the first and second night are shown in Figures 2-3. The spectra show strong Ly α and He II emission lines, both of which exhibit similar kinematic structure in the 2D spectrum. The measured fluxes and flux limits were derived separately from each night’s data using a $1.5 \times 5.0''$ aperture, chosen to maximize the signal-to-noise ratio of the He II measurement (Table 1). Faint continuum emission is detected in the spectra (Figure 3). We scaled the spectra by a factor of 1.4 and 1.6, respectively, in order to match the

continuum fluxes measured from the much deeper ND-WFS broad-band data within the region covered by the slit (Table 2).

The Ly α and He II luminosities from Night 1 are $L_{Ly\alpha} = L_{Ly\alpha,ap} \times f_{geo} \times f_{profile} \approx 5.4 \times 10^{43} \text{ erg s}^{-1}$ and $L_{HeII} = L_{HeII,ap} \times f_{geo} \approx 4.0 \times 10^{42} \text{ erg s}^{-1}$. $L_{Ly\alpha,ap} = 9.3 \times 10^{42} \text{ erg s}^{-1}$ and $L_{HeII,ap} = 1.2 \times 10^{42} \text{ erg s}^{-1}$ are the luminosities measured within the spectroscopic aperture, f_{geo} is the geometric correction factor between the spectroscopic aperture and full extent of the nebula, and $f_{profile}$ corrects for asymmetry in the Ly α profile due to blue side absorption. We discuss the estimation of these correction factors below.

The geometric correction factor f_{geo} was derived from a comparison of the spatial extent of the nebula measured in the Ly α line versus the extent in the B_W imaging. In our best seeing Night 1 data, where we have accurate spatial information and low slit losses, the Ly α is extended by $\approx 5''$ (42.3 kpc) with a fairly sharp truncation at large radii, but with a possible extension towards the west (right of center, Figure 4). The He II emission is weaker than the Ly α by a factor of 10, but it appears that at lower signal-to-noise the He II nebula extends to roughly the same radius as the core of the Ly α nebula (no westward extension). The Night 2 data show a Ly α extent of $\approx 6''$ and a He II extent of $\approx 5''$ but suffer from slit losses and degraded spatial resolution due to poor seeing and wind-shake. The extent of the Ly α nebula in the spectroscopic observations is in rough agreement with the spatial extent of the diffuse emission measured from the broad-band B_W data along the position of the slit ($\approx 6.6''$, ≈ 56 kpc above a B_W surface brightness of $4.5 \times 10^{-16} \text{ erg s}^{-1} \text{ cm}^{-2} \text{ arcsec}^{-2}$). The full area of the diffuse emission in the B_W imaging is ≈ 26 square arcseconds. Assuming that the Ly α emission is distributed similarly to the B_W continuum emission, we estimated that a geometric correction factor of $f_{geo} = 3.4$ is required to obtain the total Ly α flux from the nebula. This correction is very approximate; narrow-band imaging and/or spatially-resolved spectroscopy will be required to accurately account for the contributions of line and continuum emission to different portions of the nebula.

We derived the Ly α blue side absorption correction $f_{profile}$ using a comparison of the Ly α and He II line centroids. The Ly α profile is fairly symmetric (Figure 5), but the center of the Ly α line is offset to the red from the systemic redshift, as determined from the centroid of the He II emission line, likely due to absorption. We estimated the amount of blue side absorption of Ly α by mirroring the red side of the Ly α profile across the line centroid, and derived a factor of 1.7 (Night 1) and 1.8 (Night 2) increase in the Ly α flux. We therefore used a correction factor of $f_{profile} = 1.7$ to obtain the final Night 1 Ly α luminosity.

The nebula shows clear velocity structure in both the Ly α and He II lines. The lines are resolved, showing Ly α and He II velocity dispersions of $\sigma_v \approx 400$ and 250 km s^{-1} , respectively, corrected for the instrumental resolution. Figure 6 shows the velocity profile of the Ly α line from Night 1 and Night 2 derived using 2 pixel (0.56'') extractions. The profile is relatively smooth but flattens on the east (left) of center. The spatially-resolved Ly α velocity dispersion is essentially constant across the neb-

³ IRAF is distributed by the National Optical Astronomy Observatories, which are operated by the Association of Universities for Research in Astronomy, Inc., under cooperative agreement with the National Science Foundation.

⁴ <http://iraf.noao.edu/iraf/ftp/iraf/extern/xdimsum020627>

⁵ KPNO IRS Standard Star Manual

ula.

3.2. C IV, C III], and Ne IV] Emission

Despite the strong Ly α and He II emission seen in the Night 1 data, there is no detection of C III], C IV, or Ne IV]. The 1σ upper limits on the line ratios are C IV/He II < 0.23, C III]/He II < 0.19, and Ne IV]/He II < 0.23. Due to the excellent and stable observing conditions during Night 1, the Night 1 spectrum provides the most accurate flux measurements for Ly α and He II along with higher resolution kinematic information and the strongest limits on the C III], C IV, and Ne IV] emission from the source. In contrast, the Night 2 spectrum shows weak C III] and marginal C IV and Ne IV] emission at the same redshift. The resulting line ratios are C IV/He II = 0.36, C III]/He II < 0.82, and Ne IV]/He II < 0.49. The Night 2 data provide additional constraints on the line ratios but must be treated with care due to the Night 2 observing conditions. Due to the poor seeing and the wind-shake of the telescope, the Night 2 spectrum suffers from slit losses as well as contamination from nearby sources nominally off the slit, most importantly from a compact red source to the WNW of the target center (Source A; see Figure 1).

From a comparison of the line ratios derived from each night, we argue that the metal line emission is not from the same spatial location as the Ly α and He II, and may instead be associated with the region closer to Source A. On Night 2, the C III]/He II ratio was 0.82; thus if the emission were perfectly cospatial, we should have detected C III] on Night 1 at $\approx 5.1 \times 10^{-17}$ erg s $^{-1}$ cm $^{-2}$, roughly the same significance as He II. Instead, we can rule out C III] emission at the 4.3σ level. For Ne IV], we should have detected it at 3.0×10^{-17} erg s $^{-1}$ cm $^{-2}$ on Night 1, which disagrees at the 2.2σ level with our Night 1 result. We cannot make a robust comparison for C IV, as it is only detected at the 2σ level even on Night 2, but we make the assumption that all the metal line emission originates from the same source. In contrast, the He II/Ly α line ratios are consistent between the two nights (0.12 ± 0.04 and 0.13 ± 0.02 , respectively), indicating that the Ly α and He II are indeed cospatial within the region sampled by these observations even though the metal line emission varies spatially.

The offsets in the spatial profiles of the lines are consistent with the idea that the data from the two nights sampled different spatial regions. If the C IV, C III], and Ne IV] lines are from the region around Source A and if the wind-shake was consistently perpendicular to the slit, there should be a ≈ 5.2 pixel ($1.5''$ West) offset between the spatial centroid of these lines and that of Ly α . However, this offset will vary by an estimated $\approx \pm 3.6$ pixels ($\approx 1''$) or more depending on the direction of the telescope wind-shake relative to the angle of the slit during a given exposure. We do see a difference between the two nights when we look at the spatial profiles extracted in 2 pixel spatial bins along the spatial direction (Figure 4); the Night 1 profile is skewed towards the East (left, away from Source A), whereas the Night 2 profile is peaked closer to the position of Source A, suggesting contamination. We use these spatial profiles to compute flux-weighted mean spatial centroids for each emission line separately. The He II position is consistent with that of Ly α to within 1σ ($\Delta x = 1.41 \pm 1.54$ pixels, $0.40 \pm 0.43''$).

The C III] offset is 4.03 ± 2.07 pixels ($1.13 \pm 0.58''$) in the direction of Source A. (Due to the intrinsic faintness of the C IV and Ne IV] lines, the computed offsets are not statistically significant.) Follow-up observations will be required to resolve this issue, but it appears that the C III] line is offset from the spatial centroid of the Ly α at the 1.9σ level, in the right direction and at roughly the correct position to be explained by contamination from the region closer to Source A.

Given the pointing uncertainty and inevitability of contamination from sources off the slit due to the unstable conditions on Night 2, the discrepancy in the spatial profiles between the two nights, the evidence that the C III] line shows a spatial offset consistent with the position of Source A, and the fact that the Night 1 data are inconsistent with the fluxes of Ne IV] and C III] measured on Night 2 at $\sim 2-4\sigma$, we argue that much of the metal line emission derives from the region around Source A. We cannot rule out that some is emitted further out in the nebula, but even if it does, it arises from a region spatially distinct from the region observed on Night 1. Combining the data from the two nights would not be appropriate due to the different spatial sampling of the observations and these intrinsic spatial inhomogeneities. In the absence of more definitive data, we use the metal emission line measurements from both nights as independent upper limits on the emission coming from two possibly distinct regions of the nebula.

4. DISCUSSION

In this section we derive estimates for the physical properties of PRG1 and use photoionization models to gain insight into the gas metallicity and the possible source(s) of ionization. Despite the strong Ly α +He II signature and weak metal line emission often associated with primordial phenomena, we find that it is not possible to make an unambiguous determination of the source of ionization. The line ratios are consistent with a nebula comprised of low (but non-zero) metallicity gas, irrespective of the nature of the ionizing source, but this conclusion depends on the unknown ionization parameter of the system.

4.1. Physical Properties of the Nebula

Our discovery data can be used to put constraints on the physical properties of the nebula. Using the emission measure of Ly α , we can estimate the electron density:

$$L_{Ly\alpha} = \frac{j_{Ly\alpha}}{j_{H\beta}} n_p n_e f V h \nu_{H\beta} \alpha_{H\beta}^{eff} \quad (1)$$

$$\approx 1.2 \frac{j_{Ly\alpha}}{j_{H\beta}} n_e^2 f V h \nu_{H\beta} \alpha_{H\beta}^{eff} \quad (2)$$

where $j_{Ly\alpha}$ and $j_{H\beta}$ are the emission coefficients for Ly α and H β , respectively, n_p and n_e are the proton and electron number densities with $n_e \approx 1.2n_p$ (the factor of 1.2 accounts for the contribution of electrons from doubly-ionized Helium), f is the volume filling factor of the nebula, V is the volume of the nebula, h is Planck's constant, $\nu_{H\beta}$ is the frequency of H β , and $\alpha_{H\beta}^{eff}$ is the effective recombination coefficient for H β (Osterbrock 1989). We approximate the nebula as a sphere with radius $R \approx 28.0$ kpc. The Ly α luminosity extrapolated to the entire nebula and corrected for blue side absorption (5.4×10^{43} erg s $^{-1}$) corresponds to

an electron number density of $n_e \approx 0.094f^{-0.5} \text{ cm}^{-3} \approx 29.7(f/10^{-5})^{-0.5} \text{ cm}^{-3}$, where we have used a typical value for f derived for the line-emitting regions in cluster cooling flows ($\sim 10^{-5}$; e.g., Heckman et al. 1989). This corresponds to an ionized gas mass of $M_{ion}=1.25m_p n_e fV = 8.4 \times 10^8 (f/10^{-5})^{0.5} M_\odot$.

Similarly, the He II emission measure can be used to estimate the He $^{++}$ and electron densities, assuming the cosmic mass fraction of He:

$$L_{HeII\lambda 1640} = \frac{j_{\lambda 1640}}{j_{\lambda 4686}} n_{He^{++}} + n_e f V h \nu_{\lambda 4686} \alpha_{\lambda 4686}^{eff} \quad (3)$$

$$\approx \frac{j_{\lambda 1640}}{j_{\lambda 4686}} (14) n_{He^{++}}^2 f V h \nu_{\lambda 4686} \alpha_{\lambda 4686}^{eff} \quad (4)$$

where $j_{\lambda 1640}$ and $j_{\lambda 4686}$ are the emission coefficients, $n_{He^{++}}$ and n_e are the He $^{++}$ and electron number densities with $n_e \approx 1.2n_p \approx 14n_{He^{++}}$, $\nu_{\lambda 4686}$ is the frequency of He II $\lambda 4686$, and $\alpha_{\lambda 4686}^{eff}$ is the He II $\lambda 4686$ effective recombination coefficient (Osterbrock 1989). The He II luminosity extrapolated to the whole nebula ($4.0 \times 10^{42} \text{ erg s}^{-1}$) corresponds to a He $^{++}$ number density of $n_{He^{++}} \approx 1.0(f/10^{-5})^{-0.5} \text{ cm}^{-3}$ and an electron number density of $n_e \approx 14.5(f/10^{-5})^{-0.5} \text{ cm}^{-3}$. This corresponds to an ionized gas mass of $M_{ion}=1.25m_p n_e fV = 4.1 \times 10^8 (f/10^{-5})^{0.5} M_\odot$, roughly consistent with the Ly α estimate.

If we make the naive assumption that the velocity spread results from rotation with $V_c \approx \Delta V/2 = 350 \text{ km s}^{-1}$ at a radius of 28 kpc ($3.3''$), we estimate the mass interior to this radius to be $M_{rot} = 8.0 \times 10^{11} \sin^2 i M_\odot$, where i is the inclination of the system. If the velocity dispersion is due to random motions of small clouds within the system, we estimate the dynamical mass (using the more kinematically robust He II line; $\sigma_v = 245 \text{ km s}^{-1}$) to be $M_{rand} = 1.9 \times 10^{12} M_\odot$.

The spatial extent of the Ly α (H $^+$) and He II (He $^{++}$) emitting regions appear to be similar in size, certainly within a factor of two ($R_{H^+}/R_{He^{++}} \lesssim 2$). This is somewhat surprising when we consider a simple Strömgren sphere argument. Assuming a hard central ionizing source (an AGN or a Pop III SED) embedded within an infinite spherical H+He cloud, the predicted size ratio of the H $^+$ and He $^{++}$ -emitting regions is $R_{H^+}/R_{He^{++}} \sim 9-17$, an order of magnitude higher than we observe. This suggests that either the H $^+$ region is density-bounded, that the sources of ionization are distributed throughout the nebula, or that the assumption of spherical symmetry is invalid (e.g., the cloud is illuminated from the outside).

The observed Ly α luminosity ($L_{Ly\alpha} = 5.4 \times 10^{43} \text{ erg s}^{-1}$) corresponds to a H-ionizing photon flux ($13.6 \text{ eV} \leq E_\gamma \leq 54.4 \text{ eV}$) of:

$$Q(H) = \frac{L_{Ly\alpha}}{h\nu_{Ly\alpha}} \frac{1}{0.68} \approx 4.9 \times 10^{54} \text{ photons s}^{-1} \quad (5)$$

where we have assumed that the fraction of H ionizing photons converted into Ly α is 0.68 (Spitzer 1978). We note that this is likely a lower limit due to a number of considerations: Ly α is highly susceptible to resonant scattering and is easily destroyed by dust, and Ly α for this system is observed at $\approx 3250\text{\AA}$, a wavelength regime that suffers from very low atmospheric transmission and poor CCD sensitivity, making accurate flux calibration difficult.

From the observed He II emission ($L_{HeII} = 4.0 \times 10^{42} \text{ erg s}^{-1}$), we calculate a He $^+$ -ionizing photon flux ($E_\gamma \geq 54.4 \text{ eV}$) of:

$$Q(He^+) = \frac{L_{\lambda 1640}}{h\nu_{\lambda 1640}} \frac{\alpha_{HeII}^{eff}}{\alpha_{HeII}^{1640}} \approx 6.2 \times 10^{53} \text{ photons s}^{-1} \quad (6)$$

where $\alpha_{HeII}^{eff} = 1.53 \times 10^{-12} \text{ cm}^3 \text{ s}^{-1}$ (case B; 100 cm^{-3} , 10^4 K ; Storey & Hummer 1995) and $\alpha_{HeII}^{\lambda 1640} = \alpha_{HeII}^{4686} \frac{j_{\lambda 1640}}{j_{\lambda 4686}} \frac{\nu_{\lambda 4686}}{\nu_{\lambda 1640}} = 8.08 \times 10^{-13} \text{ cm}^3 \text{ s}^{-1}$ (case B; Osterbrock 1989).

The large value of $Q(He^+)/Q(H)=0.13$ is strong evidence that the source is illuminated by a hard ionizing continuum. The prediction for a Pop II stellar population (instantaneous burst, Salpeter IMF, 1-100 M_\odot , $Z = 0.001$; Schaerer 2003) is $Q(He^+)/Q(H) = 0.0004$; while our Ly α measurement may be compromised by radiative transfer effects and poor flux calibration at the edge of the atmospheric cut-off, it would need to have been underestimated by more than a factor of 100 in order for the observed $Q(He^+)/Q(H)$ to match that of a normal Pop II stellar population. The observed $Q(He^+)/Q(H)$ is in the range expected for AGN or Pop III stars. A typical AGN template has a ratio of $Q(He^+)/Q(H) \sim 0.09$ (Elvis et al. 1994), more consistent with the observational constraint. While normal metallicity stellar populations will have very little flux above the He $^+$ ionization edge, Pop III stars are predicted to have much harder spectra due to high temperatures, low stellar atmospheric opacity, and a top-heavy IMF. Strong mass loss from these stars would cause higher effective temperatures, boosting the hard ionizing photons even further. Schaerer (2002) calculated a suite of Pop III models, both with and without strong mass loss. For individual high mass stars ($M \geq 80-300 M_\odot$) they predict $Q(He^+)/Q(H) \geq 0.022-0.11$. Models with mass loss yields ratios of $Q(He^+)/Q(H) \geq 0.06-0.17$ ($80-300 M_\odot$). However, such large $Q(He^+)/Q(H)$ ratios persists for only a few Myrs for instantaneous burst models. Constant star-forming Pop III models (with no mass loss) integrated over a range of IMFs yield $Q(He^+)/Q(H) \leq 0.04$, and the value decreases with increasing metallicity (Schaerer 2003). There are numerous uncertainties in these estimates, but broadly speaking the observed $Q(He^+)/Q(H)$ ratio is in the range populated only by AGN and the very lowest metallicity stellar populations.

4.2. Photoionization Modeling

The ubiquity of AGN, the association of AGN and extended emission line regions (EELRs), and the presence of spatially varying metal line emission suggest that an AGN is a plausible source of ionization. At the same time, the observed line ratios are highly unusual and have been tied in the theoretical literature to primordial galaxy formation processes (the presence of Pop III stars or gravitational cooling radiation). A comparison of the line ratios from PRG1 with those of radio galaxy EELRs and other Ly α nebulae is shown in Table 3. While the Ly α /He II ratios are comparable, other than the C III]/He II ratio on Night 2, all the metal line ratios from this source are at the low end or lower than the range seen in EELRs. Furthermore, this source shows very different line ratios than those seen in another large radio-quiet Ly α nebula at $z \approx 2.7$ (Dey et al. 2005).

In order to gain greater insight into the metallicity and possible ionization sources for the nebula, we used `Cloudy`⁶ to model simple, constant density gas clouds being illuminated by AGN, Pop III, and Pop II SEDs and predict the resulting line ratios and continuum emission. The AGN template is taken from Mathews & Ferland (1987) ($F_\nu \propto \nu^{-1.0}$ at $26 < h\nu < 56$ eV, $F_\nu \propto \nu^{-3.0}$ at $56 < h\nu < 365$ eV), and the Pop III spectra are Tumlinson et al. (2006) 1 Myr models ($Z = 0$, a top-heavy IMF peaked around $10M_\odot$ with $\sigma=1.0$, i.e., their case A). The Pop II case is a 1 Myr, $Z = 0.001$, Salpeter IMF, instantaneous burst model from Starburst 99 (Leitherer et al. 1996).

The strong, spatially-extended Ly α +He II emission and weak, spatially-variable C III] and C IV emission in our discovery spectra and the blue, spatially-extended continuum emission measured from deep broad-band imaging provide constraints on the metallicity of the gas and on the slope of the ionizing continuum in the system. He⁺ and C⁺ have similar ionization potentials (54.4 eV and 47.9 eV, respectively), so a comparison of He II and C IV puts constraints on the metallicity that are less dependent on the ionizing continuum slope. The Ly α and C III] emission lines (relevant ionization potentials of H and C⁺: 13.6 eV and 24.4 eV) provide additional constraints on the slope of the ionizing continuum.

The observed lines will also depend on the ionization parameter of the system. A very rough estimate based on our discovery data is $U = \phi(H)/(n_H c) \gtrsim 0.0002$, where $\phi(H)=Q(H)/(\pi R^2)$ is the surface flux of ionizing photons, n_H is the total hydrogen gas density, and R is the radius of the cloud. We have assumed our observed quantities: $Q(H)=4.9 \times 10^{54}$ photons s⁻¹, $n_H \sim n_e \sim 29.7$ cm⁻³, and $R \approx 28$ kpc. However, this estimate is uncertain and most likely a lower limit. We have argued that the Ly α flux is likely underestimated and raised the possibility that the system is density-bounded, both of which will cause an underestimate of the ionizing photon flux (possibly by an order of magnitude). In addition, the geometry of the system is clearly complex, and the estimated density depends critically on the assumed value of the filling factor. The density estimates in Section 4.1 are larger than typical values for the ISM ($n_H \sim 1$ cm⁻³); if the cloud is in fact more similar to typical ISM densities, the ionization parameter would increase by over an order of magnitude. A more sophisticated treatment of the ionization parameter is beyond the scope of this analysis, so for the purposes of this paper we modeled a reasonable range of ionization parameters: $\text{Log } U = [-3, -1, 0]$.

4.3. Metallicity of the Gas

In order to explore the range of parameter space allowed by our observations, in Figure 7 we plot line diagnostics for models with a range of ionization parameters, metallicities, and ionizing SEDs, comparing them to our observed limits on the line ratios of the nebulosity from Night 1 and Night 2.

For low ionization parameters ($\text{Log } U < -1$), it is possible to produce the observed line ratios with an AGN SED illuminating solar metallicity gas (Figure 7; blue plus signs). For higher ionization parameter ($\text{Log } U \geq$

-1), the observed ratios require low metallicity gas. In the case of an AGN SED, the C IV/He II and C III]/He II limits imply $Z < 10^{-2} Z_\odot$. Models with Pop III ionization lead to lower metallicity estimates of $Z < 10^{-3} Z_\odot$. (For the Pop II model even lower metallicities would be required, but this case is highly unlikely given the large $Q(\text{He}^+)/Q(\text{H})$ ratio, as discussed in Section 4.1.) To put this into context, these metallicity estimates are at or below the lowest limits for weak Mg II absorbers at $0.4 < z < 2.4$ ($>10^{-2}$ - $10^{-2.5}$; Lynch & Charlton 2007). Studies of the most metal-poor damped Ly α absorbers have shown that none have metallicities lower than $[Fe/H] > -3$ (Pettini et al. 2008). Ly α forest clouds at $z \approx 3$ with $N(\text{H}) > 10^{15}$ cm⁻² are uniformly metal-enriched with carbon abundances of $\approx 10^{-2} Z_\odot$, and observations of lower column density Ly α forest clouds indicate that there may be universal minimum metallicity of $3.5 \times 10^{-4} Z_\odot$ that is roughly constant from $z \approx 2 - 6$ (Songaila 2001). If the metallicity of PRG1 is similar to the lowest metallicities measured from absorption-line studies, this would be the first time such a system has been seen in Ly α and He II emission.

While the weak metal line emission suggests a low metallicity system, the metallicity estimates are uncertain due to a variety of factors, none of which are well-constrained by the current data, e.g., the ionization parameter, the geometry of the cloud and ionizing source(s), and the intensity and spectrum of the source(s) of ionization. Putting stronger constraints on the metallicity of the nebula will require deeper spectroscopy and more detailed photoionization modeling, which is beyond the scope of the current paper.

4.4. Source of Ionization

The large He II equivalent width and large He II/Ly α ratio is strong evidence that the nebula is powered by a hard ionizing continuum. We discuss each of the possible ionization sources in turn: AGN, shock ionization, Wolf-Rayet stars, low metallicity (Pop II) and zero metallicity (Pop III) star formation, and gravitational cooling radiation.

4.4.1. AGN

An AGN can produce high He II/Ly α ratios and weaker C IV and C III] emission lines, particularly if it is illuminating a low metallicity cloud. This scenario is certainly plausible, as emission line halos (e.g., Ly α , C III], He II, C IV) around radio galaxies have been known for some time, arising predominantly from a combination of jet-ISM interactions and scattered light from the AGN or from spatially-extended star formation (e.g., McCarthy et al. 1987; van Ojik et al. 1996; Dey et al. 1997; Villar-Martín et al. 2003; Reuland et al. 2003). Unlike our Ly α +He II nebula, however, these gaseous haloes are predominantly metal-enriched, with strong C III] and C IV emission (e.g., Reuland et al. 2007; Maxfield et al. 2002).

While there is no compact source visible in the center of the nebula, there are several compact sources in the vicinity of the nebula that could in principle harbor an AGN (Figure 1). For two reasons we believe that if there is an AGN in the system, it must be at the position of Source A. First, we find that even if all the nearby sources were AGN, Source A would contribute the vast majority

⁶ Calculations were performed with version 07.02.02 of `Cloudy`, last described by Ferland et al. (1998).

of the ionizing photon flux. When we scale the standard quasar template from Elvis et al. (1994) to match the measured B_W flux from each source and calculate the corresponding ionizing photon flux, the net contribution is only 2% of the ionizing photon flux required to explain the Ly α , with nearly all of that arising from Source A. Second, in Section 3.2 we argued that the metal line emission is not cospatial with the Ly α +He II nebula, and that the observed metal lines likely derive from the region of Source A. Below we discuss the likelihood that an AGN at the position of Source A is powering the Ly α +He II nebula.

If we assume that the Night 2 metal line emission stems primarily from Source A, we can compare the measured line ratios to those of well-studied galaxy populations. At face value, the C III] and C IV emission lines associated with the region around Source A are suggestive of an AGN, however we find that the line ratios are more consistent with that seen in non-AGN LBGs (Shapley et al. 2003). The measured ratios of C IV/Ly α = 0.05 ± 0.03 and C III]/Ly α = 0.11 ± 0.02 (uncorrected for Ly α absorption) are likely upper limits due to the uncertainties in the Ly α measurement. Even so, the C IV/Ly α ratio is a factor of 4-5 lower than what is seen in LBGs flagged as narrow-line AGN (C IV/Ly α ≈ 0.25 ; Shapley et al. 2003) and in local Seyfert galaxies (C IV/Ly α ≈ 0.21 ; Ferland & Osterbrock 1986). In addition, if Ly α is underestimated by a factor of two, the corrected C IV/Ly α and C III]/Ly α ratios would match those of non-AGN LBGs. Furthermore, the ratio of C III]/C IV= 2.3 ± 1.2 is in agreement with that found for non-AGN LBGs (C III]/C IV ≈ 2.5 ; Shapley et al. 2003) and is a factor of four higher than expected from an narrow-line AGN spectrum (C III]/C IV ≈ 0.05 ; Shapley et al. 2003), suggesting Source A has a softer ionizing continuum.

There is currently no evidence from the multi-wavelength SED that Source A is an AGN. Existing X-ray coverage of the field reveals no X-ray detection at the position of the system ($F_X > 1.5 \times 10^{-14}$ erg s $^{-1}$ cm $^{-2}$ or $L_X > 2.7 \times 10^{44}$ erg s $^{-1}$, 2-7 keV observed; Kenter et al. 2005) but is too shallow to rule out lower luminosity Seyfert galaxies. The typical luminosities of Seyfert galaxies: $L_{Ly\alpha} = 10^{42} - 2 \times 10^{44}$ erg s $^{-1}$ and L_X (0.5-4.5 keV) = $5 \times 10^{42} - 10^{45}$ erg/s, with $L_{Ly\alpha}/L_X$ ratios of $\sim 0.1 - 2$ (Kriss 1984). If we combine the $L_{Ly\alpha}/L_X$ ratio as an upper limit (since the ratio for an extended nebula will be smaller due to the smaller covering fraction of the gas) with our measured Ly α luminosity (5.4×10^{43} erg s $^{-1}$), we should expect L_X (0.5-4.5 keV) $> 2.7 \times 10^{43} - 5.4 \times 10^{44}$ erg s $^{-1}$, which is at or below our current X-ray detection threshold.

The optical and MIR photometric measurements for Source A are listed in Table 2. We measured the broadband optical fluxes of Source A from NDWFS using 2.1'' diameter apertures and applied aperture corrections of [1.06, 1.40, 1.07] in the B_W , R , and I bands. The Source A IRAC photometry comes from the Spitzer Deep Wide-Field Survey (SDWFS; 3.5'' diameter aperture with point source aperture corrections of [1.38, 1.38, 1.38, 1.42]). The IRAC colors of Source A lie outside the AGN color-color selection regions of Stern et al. (2005) and Lacy et al. (2004), and the probability that an X-ray AGN will have these IRAC colors is small (Gorjian et al. 2008). The

IRAC colors of Source A are $[3.6] - [4.5] = 0.52 \pm 0.03$ (Vega) and $[5.8] - [8.0] = 0.131 \pm 0.11$ (Vega) (in "Region B" of Figure 4 of Gorjian et al. 2008). The percentage of X-ray sources down to the XBoötes limit with IRAC colors in this region is 4%. In a small portion of the survey with 10 times deeper X-ray coverage, the distribution of sources in IRAC color-color space is similar, i.e., there are very few X-ray sources with the IRAC colors of Source A (Gorjian et al. 2008). In contrast, these IRAC colors are consistent with star-forming galaxies at $z = 1.25 - 1.75$ (Donley et al. 2008), the redshift range of our source. Similarly, the IRAC SED of Source A shows the 1.6 μ m bump rather than the power-law typical of obscured AGN (Alonso-Herrero et al. 2006), indicating the MIR SED is dominated by stellar emission. All of the other sources in the vicinity show similar non-power-law SEDs.

PRG1 is also undetected at longer wavelengths: the MIPS 24 μ m non-detection corresponds to an upper limit of 51 μ Jy (1σ), and the Westerbork 20 cm survey non-detection yields a 5σ limit at 3 GHz in the restframe of 6.4×10^{23} W Hz $^{-1}$ (de Vries et al. 2002), well below the realm of high redshift radio galaxies ($\sim 10^{26}$ W Hz $^{-1}$; Seymour et al. 2007).

On the other hand, the energetics of the nebula suggest that an AGN at the projected position of Source A could explain the observed continuum emission if the AGN is highly obscured to our line-of-sight. If we make the assumption that an AGN at Source A is powering the He II emission, we can estimate the amount of B_W continuum emission we expect from the nebula due to illumination by the AGN. Scaling a standard AGN template (Elvis et al. 1994) to match the ionizing photon flux implied by the He II ($Q(\text{He}^+) \approx 6.2 \times 10^{53}$ photons s $^{-1}$), we estimate that the B_W luminosity from the AGN striking the cloud should be $L_{B_W, \text{incident}} \approx 1.9 \times 10^{41}$ erg s $^{-1}$ \AA^{-1} . This incident AGN continuum flux – the maximum possible contribution from the AGN to the observed continuum emission – is roughly the same as the measured B_W continuum emission from the nebula ($L_{B_W, \text{nebula}} \approx 1.1 \times 10^{41}$ erg s $^{-1}$ \AA^{-1}). In reality, the continuum observed within the nebula will arise solely from two-photon (2γ) continuum and scattering of AGN light with no contribution directly from the AGN itself. Given the predicted He II equivalent width from our Cloudy models of AGN illumination, we estimate the expected B_W two-photon continuum within the nebula to be $L_{B_W, 2\gamma} \approx 2.0 \times 10^{40}$ erg s $^{-1}$, roughly 18% of the observed B_W continuum of the nebula. Electron scattering of AGN light is expected to have a scattering optical depth of $\tau = n_e l \sigma_T = 0.1 - 1.1$, where $n_e \approx 1 - 10$ cm $^{-3}$ and $l = 56$ kpc is the approximate path through the nebula, corresponding to a Thompson scattering continuum of $L_{B_W, \text{Thompson}} \lesssim 1.9 \times 10^{41}$ erg s $^{-1}$ $\text{\AA}^{-1} \times (1 - e^{-\tau}) = 1.3 \times 10^{41}$ erg s $^{-1}$ \AA^{-1} , comparable to the observed B_W continuum emission. Although dust scattering, which is much more efficient than Thompson scattering, may contribute as well, large quantities of dust would be difficult to reconcile with the large observed Ly α and He II luminosities. Questions remain, but given the limitations of our discovery data it appears that an AGN at the position of Source A that is unobscured along the line-of-sight to the nebula, but

completely hidden from our viewpoint, could explain the observed B_W continuum emission. Correcting for the maximal (since we are assuming the projected separation) solid angle subtended by the cloud as seen from the Source A ($d\Omega \approx 3.1$ steradians), we find that the minimum intrinsic AGN luminosity needed to produce this incident flux is $L_{B_W, min(AGN)} \gtrsim 1.9 \times 10^{41} \text{ erg s}^{-1} \times 4\pi/d\Omega$ $\text{erg s}^{-1} \text{ \AA}^{-1} \approx 7.6 \times 10^{41} \text{ erg s}^{-1} \times \text{\AA}^{-1}$. Source A has a B_W luminosity of $1.8 \times 10^{40} \text{ erg s}^{-1} \times \text{\AA}^{-1}$, which is over an order of magnitude fainter than this firm lower limit. The AGN would therefore need to be very highly obscured along our line-of-sight to match the existing observational constraints.

In conclusion, an AGN at the position of Source A is a plausible source of the hard ionizing radiation. However, there is no visible AGN in the vicinity of the nebula, so it would have to be highly obscured along our line-of-sight. An AGN in the vicinity of the nebula must be in a radio-quiet phase and so highly obscured that even the observed MIR SED is dominated by light from the host galaxy. Deep optical and near-infrared spatially-resolved spectroscopy will be required to resolve this issue.

4.4.2. Shocks

The observed ratios are inconsistent with shock ionization in solar metallicity gas, which typically produces much higher C III]/He II and C IV/C III] ratios (e.g., ~ 3 -25 and ~ 1 -10 for shock velocities of 500-150 km s^{-1} ; Dopita & Sutherland 1996) along with strong N V] λ 1240. Stronger shock velocities are inconsistent with the narrow width of the He II line ($v_{FWHM} \lesssim 500 \text{ km s}^{-1}$).

4.4.3. Wolf-Rayet Stars

Strong He II emission is seen in both of the major classes of Wolf-Rayet stars (WN and WC), but it is accompanied by strong Si IV, N V], and/or other metal emission lines. WN stars show strong Si IV] λ 1393,1402 relative to He II, C IV, and C III], which we can rule out with our discovery spectra. WC stars usually show C IV/C III] ratios greater than 1, medium-strength Si IV, and a large number of other metal lines (e.g., Fe), all of which are inconsistent with our observations. The spectrum of a typical ‘W-R galaxy’ (a galaxy with spectrum dominated by Wolf-Rayet features) effectively averages over hundreds or thousands of W-R stars, but none-the-less typically shows Si IV, C IV, He II, and N V] emission with P-Cygni profiles due to the effects of strong stellar winds (e.g., Leitherer et al. 1996). The composite Lyman Break Galaxy (LBG) spectrum measured at $z \sim 3$ also shows Si IV and C IV with P-Cygni profiles from the stellar winds of massive stars, as well as broad He II ($v_{FWHM} \sim 1500 \text{ km s}^{-1}$), which the authors argue is most likely due to the fast, dense winds of Wolf-Rayet stars (Shapley et al. 2003). In our case, the narrow width of the He II line ($v_{FWHM} \lesssim 500 \text{ km s}^{-1}$) and the absence of other important Wolf-Rayet features (e.g., Si IV, N V]) rules out the idea that the He II emission is coming from Wolf-Rayet stars.

4.4.4. Population II Star Formation

The existence of diffuse, blue continuum that is co-spatial with the Ly α and He II line emission (Figures 1) is suggestive of a distributed source of ionization such

as spatially-extended star formation. However, the observed He II/Ly α line ratio is inconsistent with ionization by a standard Population II SED (e.g., $Z = 0.001 = 1/20Z_\odot$). The expected Q(He⁺)/Q(H) ratio for a Pop II model is several orders of magnitude lower than observed (Schaerer 2003). Predictions from our Cloudy models indicate that the dearth of hard ionizing photons translates into negligible He II emission and He II/Ly α ratios that are a factor of 1000 lower than observed. Furthermore, the large observed He II equivalent width can only be produced by very low metallicity stellar populations (Schaerer 2003).

4.4.5. Population III Star Formation

The only way to explain strong He II emission with ionization from a stellar population is to invoke very young ages and very low metallicities. The rest-frame equivalent width of Ly α ($EW \approx 294 \text{ \AA}$) is higher than or comparable to what is expected from solar metallicity and Pop II stellar populations (Schaerer 2003), but it is by no means the largest observed in Ly α -emitting galaxy surveys ($EW_{max} \gtrsim 300 \text{ \AA}$; Dawson et al. 2007). The measured equivalent width of He II, however, is very large ($EW \approx 37 \text{ \AA}$) in the context of stellar populations and only consistent with the youngest ($\lesssim 2$ Myr) and lowest metallicity stars ($\lesssim 10^{-7} Z_\odot$), in the absence of mass loss (Schaerer 2003). Here we chose a Pop III model with a moderately top-heavy IMF from Tumlinson et al. (2006) that has a peak at $10 M_\odot$ (their case A); a more top-heavy IMF will tend to boost the He II/Ly α ratio due to the additional hard ionizing photons. The ionizing photon flux implied by the Ly α and He II measurements from PRG1 implies a Pop III cluster mass of 13 - $100 \times 10^6 M_\odot$ and a B_W continuum flux of $L_{B_W, incident} \approx 1.7 \times 10^{41} \text{ erg s}^{-1} \text{ \AA}^{-1}$, roughly equal to the observed continuum ($L_{B_W, nebula} \approx 1.1 \times 10^{41} \text{ erg s}^{-1} \text{ \AA}^{-1}$). In comparing with our Cloudy models, however, we find that the observed He II/Ly α ratio (≈ 0.12) is much higher than expected from our Pop III model (≈ 0.004). However, it is important to keep in mind that model uncertainties, such as the assumed IMF and the effects of mass loss, could have a large effect on the predicted line luminosities. In addition, the possible underestimation of the Ly α flux discussed in Section 4.1 as well as a density-bounded geometry will tend to boost the observed He II/Ly α ratio.

On the face of it, it would be surprising to find such low metallicity star formation at such a low redshift. However, we cannot conclusively rule out the Pop III scenario on this basis alone. While the mean metallicity of the Universe increases with time, several theoretical models of Pop III star formation have suggested that significant metallicity inhomogeneities may exist even at low redshifts (Tornatore et al. 2007). These models predict that while the metallicity is quickly enriched at the center of collapsed structures, low metallicity regions can persist on the periphery over longer timescales, allowing Pop III star formation to proceed well after the epoch of reionization (Tornatore et al. 2007; Scannapieco et al. 2003). At $z \approx 2.3$ (roughly the redshift midpoint of our Ly α nebula survey), Tornatore et al. (2007) predict a Pop III SFR density of $1.3 \times 10^{-7} M_\odot \text{ yr}^{-1} \text{ Mpc}^{-3}$. If we were to assume that this Ly α +He II nebula is powered by very

low metallicity star formation, use the Ly α line emission (extrapolated to the entire nebula and corrected for absorption) to estimate a SFR ($\text{SFR} = L_{\text{Ly}\alpha} / 1.26 \times 10^{42} \approx 5.4 \times 10^{43} / 1.26 \times 10^{42} \text{ erg s}^{-1} \approx 42.9 M_{\odot} \text{ yr}^{-1}$; Kennicutt 1998), and ignore any incompleteness of our survey, we would calculate that one nebula of this kind within our survey volume ($1.3 \times 10^8 \text{ Mpc}^3$), corresponds to a Pop III SFR density of $\sim 3.3 \times 10^{-7} M_{\odot} \text{ yr}^{-1} \text{ Mpc}^{-3}$. This very rough estimate based on a single source is of the same order of magnitude as the model predictions (within a factor of 3) despite the large theoretical uncertainties in the conditions regulating Pop III star formation and IGM enrichment at all redshifts.

In reality, the amount of low metallicity gas and Pop III star formation as a function of redshift will depend on the efficiency of star formation in different environments and the efficiency with which stars pollute their environment, i.e., the feedback efficiency. A more realistic treatment of galactic winds in cosmological simulations (e.g., momentum-driven winds; Oppenheimer & Davé 2006) is shown to suppress the metallicity in all gas phases relative to the constant wind scenario similar to that used in Tornatore et al. (2007), which may in turn increase the fraction of Pop III star formation at any given redshift. On the other hand, only a few stellar generations would be required to produce the mass of carbon in the nebula. Assuming the derived ionized gas mass ($\sim 8 \times 10^8 M_{\odot}$), the simulated yields for Pop III supernovae ($\sim 0.2\text{-}1 M_{\odot} \text{ C}$ per $20\text{-}40 M_{\odot}$ supernova progenitor; Tominaga et al. 2007) and instantaneous mixing, enriching the cloud to $z \approx 10^{-3} Z_{\odot}$ would only require of order 750 supernovae ($2 - 4 \times 10^4 M_{\odot}$). This is several orders of magnitude lower than the fraction of the cluster mass implied by the Ly α and He II luminosities that is in stars with $M > 20 M_{\odot}$ for the assumed top-heavy IMF: $f(M > 20 M_{\odot}) = 0.26$ or $3 - 27 \times 10^6 M_{\odot}$. Thus it is likely the nebula would be polluted to the observed levels over a relatively short timescale.

Large uncertainties remain in our understanding of Pop III star formation. The expected fraction of Pop III star formation at a give epoch is unclear, feedback efficiency of these first stars is largely unconstrained, and there are a wide range of possible Ly α /He II ratios, depending on stellar mass loss, star formation history, and the complicated effects of Ly α radiative transfer. Despite the strong Ly α +He II signature in this source, we cannot conclusively confirm or rule out Pop III star formation as a source of ionization with the current observations.

4.4.6. Gravitational Cooling Radiation

A number of theoretical papers have addressed the issue of gravitational cooling radiation, i.e., the cooling of gas as it collapses within the dark matter potential and heats to $T \approx 10^4 \text{ K}$. Metal-line cooling is possible for gas with $T < 10^4 \text{ K}$, but it is ~ 1000 times less efficient than cooling via Ly α emission, unless $Z > 0.1 Z_{\odot}$ (Haiman et al. 2000). Thus for low metallicity gas, strong Ly α emission is expected to dominate the cooling (Fardal et al. 2001). He II emission may be important as well, but its contribution relative to Ly α is unclear due to uncertainties in how much Ly α will escape the system. From a semi-analytic calculation assuming monolithic collapse, Haiman et al. (2000) suggested that a cloud that is sufficiently metal-poor

will radiate 10% of the energy via He II $\lambda 304\text{\AA}$; this corresponds to a He II $\lambda 1640/\text{Ly}\alpha$ of ~ 0.01 , where we have followed Yang et al. (2006) and adopted a ratio of He II $\lambda 1640/\text{He II } \lambda 304 \approx 0.10$, i.e., the case B values of Storey & Hummer (1995) extrapolated to the low density limit. Using Parallel TreeSPH simulations, Yang et al. (2006) predicted ratios of He II $\lambda 1640/\text{Ly}\alpha \lesssim 0.10 - 0.001$ for gravitationally cooling clouds, depending on the degree to which self-shielding of the gas reduces the Ly α flux. This range approaches the observed ratio for PRG1, but due to subsequent corrections to the treatment of star-forming gas in more recent simulations the predictions from Yang et al. (2006) are likely overestimates (Y. Yang 2008, private communication). Thus, the observed He II/Ly α ratio appears to be higher than predicted for gravitational cooling radiation, but again the uncertainties in both the theoretical predictions and in our Ly α measurement make it difficult to draw firm conclusions.

Some of the theoretical predictions for gravitationally cooling clouds are consistent with our observations. The observed He II line width ($\sigma_v < 250 \text{ km s}^{-1}$) is more consistent with gravitational cooling radiation ($\sigma_v < 400 \text{ km s}^{-1}$; e.g., Yang et al. 2006) than with outflows. In addition, theoretical simulations of the redshift evolution predict a peak in the number density of gravitational cooling Ly α nebulae at $z \approx 2$, consistent with our discovery of a Ly α +He II nebula at $z \approx 1.7$. While Dijkstra (2007) predicts rest-frame Ly α equivalent widths of $> 1000\text{\AA}$ for gravitationally cooling clouds, he notes that the observed rest-frame equivalent width is likely to be reduced by a factor of 5-10 due to scattering of Ly α photons in the intergalactic medium, more in line with our measurements.

However, a number of other theoretical predictions of gravitational cooling radiation do not fit our observations. First, the simulations do not reproduce the relative sizes of the observed Ly α and He II regions. Fardal et al. (2001) could not reproduce the sizes of the largest observed Ly α nebulae unless they invoked resonant scattering of the Ly α emission. In that case, the He II emission should be more centrally-concentrated than the Ly α . Similarly, Yang et al. (2006) suggested that He II regions would likely be too small to resolve with current observational facilities. In contrast, in our Ly α +He II nebula the He II region appears to be comparable in size to the Ly α region ($\approx 45 \text{ kpc}$). The theoretical papers also predict that Ly α nebulae will only be present as a halo around a massive galaxy (Fardal et al. 2001; Furlanetto et al. 2005). While there are a few faint sources around the edge of our nebula, and there may be unresolved low surface brightness clumps within the cloud, the multi-wavelength imaging shows no evidence for a central massive galaxy in this system.

Given the uncertainties in the theoretical predictions and the limits of our discovery data it is difficult to assess the applicability of the gravitational cooling model. The weight of the current evidence disfavors gravitational cooling as the sole explanation for the line emission, but it is certainly possible that the nebula is powered by multiple processes, with gravitational cooling radiation playing a larger role on the outskirts and photoionization from stars or AGN dominating the ionization of the

central regions.

5. IMPLICATIONS

Strong Ly α +He II in the absence of strong metal lines has been championed as a unique observational signature of primordial galaxy formation (e.g., Pop III star formation or gravitationally cooling clouds), but the discovery of this Ly α +He II nebula suggests that the situation can be much more complex in actual astrophysical sources. Occam’s razor suggests that the most likely power source is an AGN at the position of Source A. An analysis of the existing data shows no obvious evidence of a powerful AGN in the vicinity, so to explain the ionization of the nebula, an AGN would need to be highly obscured even in the mid-infrared. The line ratios rule out ionization by shocks, Wolf-Rayet stars, and Pop II star formation. Pop III star formation would provide the necessary hard ionizing continuum to explain the observed line ratios along with a natural explanation for the spatially-extended continuum emission, but this scenario appears unlikely given the low redshift. Despite the compelling Ly α +He II signature, the complexity of this source and the large uncertainties in theoretical predictions preclude a more definitive conclusion. The contribution from gravitational cooling radiation is similarly unclear, although the morphology of the nebula (with no central compact source) and relative sizes of the Ly α and He II emitting regions disfavor this hypothesis as a dominant mechanism.

One of the most important implications of this discovery is that it demonstrates we must be careful when using strong Ly α +He II emission as a tracer of Pop III star formation. Surveys looking specifically for this Ly α +He II signature are ongoing. While the low redshift of PRG1 allows for the detailed multi-wavelength follow-up necessary in order to understand the power source and the metallicity of the gas, the same cannot be said for ongoing Ly α +He II emitter surveys at higher redshift that will lack longer wavelength coverage and be sensitivity-challenged. It is extremely important to note that if this Ly α +He II had been discovered at high redshift, it would have been easy to jump prematurely to the Pop III conclusion. The discovery of a Ly α +He II nebula at $z \approx 1.67$ therefore provides an ideal opportunity to evaluate the extent to which strong Ly α +He II emission can be used as a unique tracer of Pop III star formation and underscores the importance of using care when interpreting a strong Ly α +He II signature in the absence of more extensive multi-wavelength data.

6. SUMMARY

We have discovered a Ly α nebula at $z \approx 1.67$ (the lowest redshift Ly α nebula known) that shows strong, diffuse He II emission and weak/negligible C III] and C IV emission. From the line ratios we derive evidence that this

nebula may contain low metallicity ($Z < 10^{-2} - 10^{-3} Z_{\odot}$) gas, depending on the unknown ionization parameter, that is being illuminated by a hard ionizing continuum, either due an AGN or a very low metallicity stellar population (Pop III), by gravitational cooling, or some combination thereof. The softer continua of Population I and II stars can be conclusively ruled out along with ionization by shocks and Wolf-Rayet stars. No obvious, unobscured, powerful AGN is seen in the system; thus if an AGN is responsible, it must be highly obscured along our line-of-sight. Despite the strong Ly α +He II signature, our detailed analysis of the discovery data shows that dedicated follow-up observations will be required in order to draw firm conclusions about the dominant source of ionization for the nebula and better constrain the metallicity. This is the first time that the predicted observational signature of very low metallicity (Pop III) star formation – strong Ly α and He II in the absence of strong metal lines – has been seen in a spatially-extended source; however, the complex nature of the nebula and the fact that such complexity becomes increasingly difficult to discern with redshift suggest that studies at high redshift will need to use caution when interpreting future Ly α +He II discoveries.

We are grateful to J. Tumlinson for providing the Pop III evolving spectra, to E. Le Floch and the IRS GTO and MIPS GTO teams for providing the MIPS data, to Gary Ferland for useful advice on the photoionization modeling, and to K. Finlator for observing assistance and many helpful discussions. D. Stern, M. Ashby, M. Brodwin, and the rest of the SDWFS team are thanked for access to the most current Spitzer IRAC imaging of the Boötes field. We also thank the anonymous referee for suggestions that improved the clarity of this paper. We would like to acknowledge the expert assistance of the staff of the MMT Observatory (especially John McAfee, Ale Milone, and G. Grant Williams). M. P. was supported by an NSF Graduate Research Fellowship and a P.E.O Scholar Award. This research builds on data from the NOAO Deep Wide-Field Survey (NDWFS) as distributed by the NOAO Science Archive. NOAO is operated by the Association of Universities for Research in Astronomy (AURA), Inc. under a cooperative agreement with the National Science Foundation. Some of the data presented in this paper were obtained from the Multimission Archive at the Space Telescope Science Institute (MAST). STScI is operated by the Association of Universities for Research in Astronomy, Inc., under NASA contract NAS5-26555. Support for MAST for non-HST data is provided by the NASA Office of Space Science via grant NAG5-7584 and by other grants and contracts.

REFERENCES

- Alonso-Herrero, A., et al. 2006, *ApJ*, 640, 167
 Bromm, V., Kudritzki, R. P., & Loeb, A. 2001, *ApJ*, 552, 464
 Dawson, S., et al. 2004, *ApJ*, 617, 707
 Dawson, S., Rhoads, J. E., Malhotra, S., Stern, D., Wang, J., Dey, A., Spinrad, H., & Jannuzi, B. T. 2007, *ApJ*, 671, 1227
 Dey, A., van Breugel, W., Vacca, W. D., & Antonucci, R. 1997, *ApJ*, 490, 698
 Dey, A., et al. 2005, *ApJ*, 629, 654
 Dijkstra, M. 2007, *ArXiv e-prints*, 711, arXiv:0711.2698
 di Serego Alighieri, S., Kurk, J., Ciardi, B., Cimatti, A., Daddi, E., & Ferrara, A. 2008, *ArXiv e-prints*, 807, arXiv:0807.4634
 Donley, J. L., Rieke, G. H., Perez-Gonzalez, P. G., & Barro, G. 2008, *ArXiv e-prints*, 806, arXiv:0806.4610
 Dopita, M. A., & Sutherland, R. S. 1996, *ApJS*, 102, 161

TABLE 1
PRG1 SPECTROSCOPIC MEASUREMENTS

	Ly α λ 1216	Nv λ 1240	Siv λ 1398	Civ λ 1549	HeII λ 1640	CIII] λ 1909	NeIV λ 2424
Night 1 - UT 2008 June 08							
Flux ^a [10 ⁻¹⁷ erg s ⁻¹ cm ⁻²]	49.9 \pm 5.7	< 6.4 ^b	< 1.8 ^b	< 1.4 ^b	6.2 \pm 1.7	< 1.2 ^b	< 1.4 ^b
EW _{rest} [Å]	294.1 \pm 39.4	-	-	-	36.8 \pm 10.1	-	-
λ_{obs} [Å]	3250.07 \pm 0.56	-	-	-	4383.07 \pm 1.25	-	-
Redshift	1.6735 \pm 0.0005	-	-	-	1.6714 \pm 0.0008	-	-
FWHM _{obs} [Å]	10.20 \pm 0.82	-	-	-	8.41 \pm 3.23	-	-
FWHM [km s ⁻¹]	941.5 \pm 75.5	-	-	-	575.5 \pm 221.1	-	-
Night 2 - UT 2008 June 09							
Flux ^a [10 ⁻¹⁷ erg s ⁻¹ cm ⁻²]	43.6 \pm 4.0	< 5.5 ^b	< 1.1 ^b	2.1 \pm 1.1	5.7 \pm 0.9	4.7 \pm 0.8	2.8 \pm 1.0
EW _{rest} [Å]	257.1 \pm 29.4	-	-	12.4 \pm 6.5	33.9 \pm 6.1	28.0 \pm 5.3	29.9 \pm 11.3
λ_{obs} [Å]	3249.59 \pm 0.38	-	-	4142.30 \pm 1.46	4381.92 \pm 0.76	5095.26 \pm 0.10	6476.81 \pm 1.83
Redshift	1.6731 \pm 0.0003	-	-	1.6724 \pm 0.0009	1.6707 \pm 0.0005	1.6695 \pm 0.0001	1.6720 \pm 0.0008
FWHM _{obs} [Å]	9.75 \pm 0.71	-	-	-	6.36 \pm 0.64	23.28 \pm 1.94	-
FWHM [km s ⁻¹]	900.4 \pm 65.1	-	-	-	435.5 \pm 44.1	1370.7 \pm 114.5	-

^a Flux measured in a 1.5 \times 5.0'' aperture. No correction has been applied for Ly α absorption. ^b Quoted upper limits are 1 σ values.

- de Vries, W. H., Morganti, R., Röttgering, H. J. A., Vermeulen, R., van Breugel, W., Rengelink, R., & Jarvis, M. J. 2002, *AJ*, 123, 1784
- Elvis, M., et al. 1994, *ApJS*, 95, 1
- Ezer, D., & Cameron, A. G. W. 1971, *Ap&SS*, 14, 399
- Fardal, M. A., Katz, N., Gardner, J. P., Hernquist, L., Weinberg, D. H., & Davé, R. 2001, *ApJ*, 562, 605
- Ferland, G. J., & Osterbrock, D. E. 1986, *ApJ*, 300, 658
- Ferland, G. J., Korista, K. T., Verner, D. A., Ferguson, J. W., Kingdon, J. B., & Verner, E. M. 1998, *PASP*, 110, 761
- Finkelstein, S. L., Rhoads, J. E., Malhotra, S., Grogan, N., & Wang, J. 2008, *ApJ*, 678, 655
- Furlanetto, S. R., Schaye, J., Springel, V., & Hernquist, L. 2005, *ApJ*, 622, 7
- Geach, J. E., Smail, I., Chapman, S. C., Alexander, D. M., Blain, A. W., Stott, J. P., & Ivison, R. J. 2007, *ApJ*, 655, L9
- Gorjian, V., et al. 2008, *ApJ*, 679, 1040
- Haiman, Z., Spaans, M., & Quataert, E. 2000, *ApJ*, 537, L5
- Heckman, T. M., Baum, S. A., van Breugel, W. J. M., & McCarthy, P. 1989, *ApJ*, 338, 48
- Humphrey, A., Villar-Martín, M., Vernet, J., Fosbury, R., di Serego Alighieri, S., & Binette, L. 2008, *MNRAS*, 383, 11
- Jannuzi, B. T., & Dey, A. 1999, in *ASP Conf. Ser. 191, Photometric Redshifts and the Detection of High Redshift Galaxies*, ed. R. Weymann et al. (San Francisco: ASP), 111
- Kennicutt, R. C., Jr. 1998, *ApJ*, 498, 541
- Kenter, A., et al. 2005, *ApJS*, 161, 9
- Kriss, G. A. 1984, *ApJ*, 277, 495
- Lacy, M., et al. 2004, *ApJS*, 154, 166
- Leitherer, C., Vacca, W. D., Conti, P. S., Filippenko, A. V., Robert, C., & Sargent, W. L. W. 1996, *ApJ*, 465, 717
- Lynch, R. S., & Charlton, J. C. 2007, *ApJ*, 666, 64
- Malhotra, S., & Rhoads, J. E. 2002, *ApJ*, 565, L71
- Martin, D. C., et al. 2005, *ApJ*, 619, L1
- Mathews, W. G., & Ferland, G. J. 1987, *ApJ*, 323, 456
- Matsuda, Y., Iono, D., Ohta, K., Yamada, T., Kawabe, R., Hayashino, T., Peck, A. B., & Petitpas, G. R. 2007, *ApJ*, 667, 667
- Maxfield, L., Spinrad, H., Stern, D., Dey, A., & Dickinson, M. 2002, *AJ*, 123, 2321
- McCarthy, P. J., Spinrad, H., Djorgovski, S., Strauss, M. A., van Breugel, W., & Liebert, J. 1987, *ApJ*, 319, L39
- Nagao, T., Motohara, K., Maiolino, R., Marconi, A., Taniguchi, Y., Aoki, K., Ajiki, M., & Shioya, Y. 2005, *ApJ*, 631, L5
- Nagao, T., et al. 2008, *ApJ*, 680, 100
- Nilsson, K. K., Fynbo, J. P. U., Møller, P., Sommer-Larsen, J., & Ledoux, C. 2006, *A&A*, 452, L23
- Oppenheimer, B. D., & Davé, R. 2006, *MNRAS*, 373, 1265
- Osterbrock, D. E. 1989, *Research supported by the University of California, John Simon Guggenheim Memorial Foundation, University of Minnesota, et al. Mill Valley, CA, University Science Books*, 1989, 422 p.
- Ouchi, M., et al. 2008, *ApJS*, 176, 301
- Pettini, M., Zych, B. J., Steidel, C. C., & Chaffee, F. H. 2008, *MNRAS*, 385, 2011
- Reuland, M., et al. 2003, *ApJ*, 592, 755
- Reuland, M., et al. 2007, *AJ*, 133, 2607
- Rhoads, J. E., et al. 2003, *AJ*, 125, 1006
- Saito, T., Shimasaku, K., Okamura, S., Ouchi, M., Akiyama, M., Yoshida, M., & Ueda, Y. 2008, *ApJ*, 675, 1076
- Scannapieco, E., Schneider, R., & Ferrara, A. 2003, *ApJ*, 589, 35
- Schaerer, D. 2002, *A&A*, 382, 28
- Schaerer, D. 2003, *A&A*, 397, 527
- Schaerer, D. 2008, *arXiv:0809.1988*
- Seymour, N., et al. 2007, *ApJS*, 171, 353
- Shapley, A. E., Steidel, C. C., Pettini, M., & Adelberger, K. L. 2003, *ApJ*, 588, 65
- Smith, D. J. B., & Jarvis, M. J. 2007, *MNRAS*, 378, L49
- Smith, D. J. B., Jarvis, M. J., Lacy, M., & Martínez-Sansigre, A. 2008, *MNRAS*, 380, 870
- Songaila, A. 2001, *ApJ*, 561, L153
- Spitzer, L. 1978, *New York Wiley-Interscience*, 1978. 333 p.
- Stern, D., et al. 2005, *ApJ*, 631, 163
- Storey, P. J., & Hummer, D. G. 1995, *MNRAS*, 272, 41
- Tominaga, N., Umeda, H., & Nomoto, K. 2007, *ApJ*, 660, 516
- Tornatore, L., Borgani, S., Dolag, K., & Matteucci, F. 2007, *MNRAS*, 382, 1050
- Tumlinson, J., Giroux, M. L., & Shull, J. M. 2001, *ApJ*, 550, L1
- Tumlinson, J. et al. 2006, *ApJ*, 641, 1
- van Ojik, R., Roettgering, H. J. A., Carilli, C. L., Miley, G. K., Bremer, M. N., & Macchetto, F. 1996, *A&A*, 313, 25
- Villar-Martín, M., Vernet, J., di Serego Alighieri, S., Fosbury, R., Humphrey, A., Pentericci, L., & Cohen, M. 2003, *New Astronomy Review*, 47, 291
- Yang, Y., Zabludoff, A. I., Davé, R., Eisenstein, D. J., Pinto, P. A., Katz, N., Weinberg, D. H., & Barton, E. J. 2006, *ApJ*, 640, 539

TABLE 2
PRG1 PHOTOMETRIC MEASUREMENTS

	Nebula ^{a,b} 10 ⁻³⁰ erg s ⁻¹ cm ⁻² Hz ⁻¹	Source A ^c 10 ⁻³⁰ erg s ⁻¹ cm ⁻² Hz ⁻¹
<i>B_W</i>	3.58 ± 0.24	2.07 ± 0.14
<i>R</i>	4.03 ± 0.49	4.60 ± 0.33
<i>I</i>	6.62 ± 0.88	8.35 ± 0.47
3.6μm	-	466.56 ± 34.13
4.5μm	-	488.70 ± 32.40
5.8μm	-	329.67 ± 31.40
8.0μm	-	194.13 ± 25.60

^a Flux measured within the same 1.5×5.0'' aperture as the spectroscopic measurements. ^b The contribution of line emission for Night 1 (Night 2): He II contributes 8% (7%) and C IV < 2% (3%) of the *B_W* emission, and Ne IV] contributes < 2% (6.5%) of the *R*-band emission. We see no contribution from line emission out to the middle of the *I*-band (8300Å, the extent of our spectroscopic coverage). ^c Optical *B_W*, *R*, and *I* fluxes were measured within 2.1'' diameter apertures. Mid-infrared fluxes (3.6, 4.5, 5.8, 8.0 μm) were measured within 3.5'' diameter apertures. Aperture corrections are discussed in the text.

TABLE 3
EMISSION LINE RATIO COMPARISON

	Lyα/HeII ^a	CIV/HeII	CIII]/HeII	CIV/CIII]	Reference
Radio Galaxy Halos (Composite)	11.7	1.75	0.73	2.4	Humphrey et al. 2008 ^b
Radio Galaxy Halos (Mean)	9.80 ± 5.69	1.59 ± 0.56	1.06 ± 1.05	2.22 ± 1.17	Humphrey et al. 2008
Stacked Lyα Blobs at <i>z</i> ≈ 3	11.11 ± 9.88	-	-	-	Saito et al. 2008
Lyα Blob at <i>z</i> ≈ 2.7	7.62 ± 0.08	1.02 ± 0.01	0.12 ± 0.02	8.34 ± 1.67	Dey et al. 2005
PRG1 Night 1	8.00 ± 2.32	< 0.22 ^c	< 0.19 ^c	-	This study
PRG1 Night 2	7.59 ± 1.43	0.36 ± 0.20	0.83 ± 0.20	0.44 ± 0.24	This study

^a No correction has been applied for Lyα absorption. ^b Errors on line ratios from composite spectrum not given. ^c 1σ upper limits.

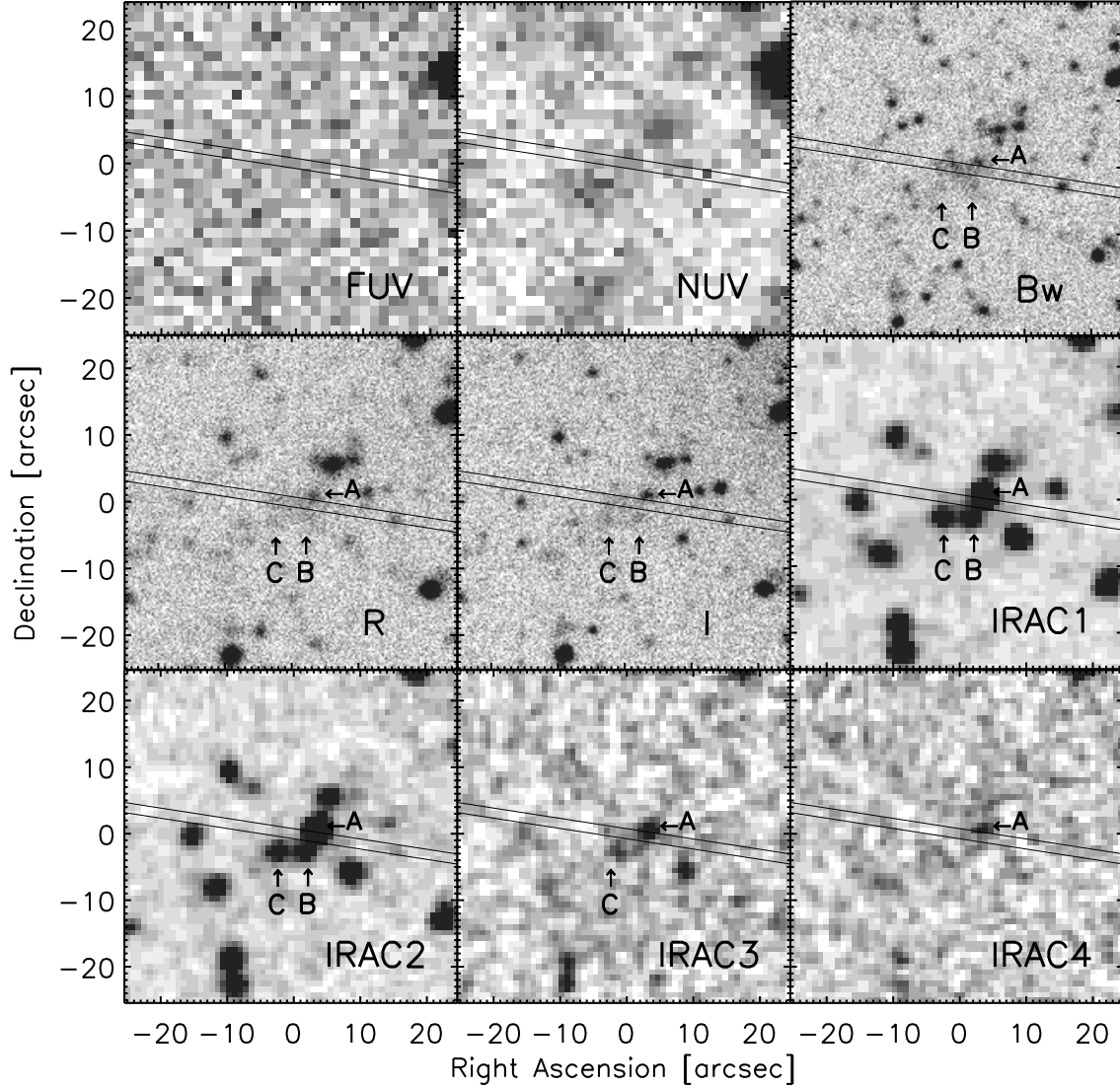


FIG. 1.— GALEX (*FUV* and *NUV*), NDWFS broad-band optical (*B_w*, *R*, and *I*), and IRAC ($3.6\mu\text{m}$, $4.5\mu\text{m}$, $5.8\mu\text{m}$, and $8.0\mu\text{m}$) postage stamps for PRG1. Images are all $1'$ on a side and centered on the coordinate location $14:35:12.439 +35:11:07.16$ (J2000). The spectroscopic slit is shown with a position angle of 81.2° . PRG1 was selected as a Ly α nebula candidate due to the diffuse blue emission in the *B_w* imaging. However, in this case Ly α is in fact outside the *B_w* band; the *B_w* flux is instead dominated by diffuse continuum and He II emission. The diffuse blue continuum emission is clearly visible in the NDWFS *B_w*-band imaging. Several compact sources in the near vicinity of the nebula have IRAC counterparts, labeled A, B, and C.

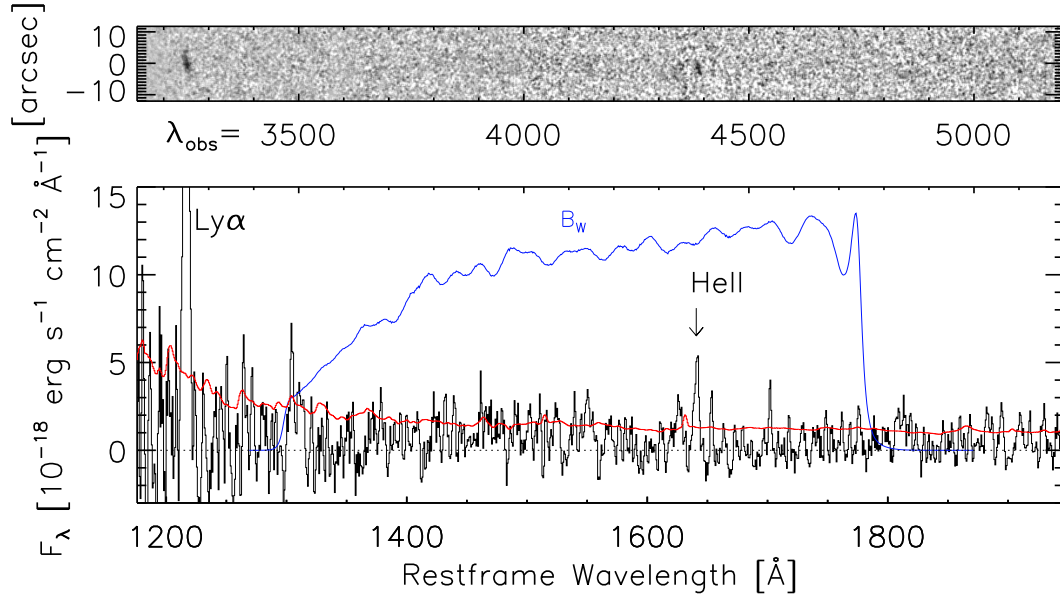


FIG. 2.— Night 1 (UT 2008 June 08) 2D and 1D spectra showing strong Ly α and He II emission from a single half hour exposure ($1.5 \times 5.0''$ aperture). The spectra have been smoothed by $0.84''$ spatially and by 5.8 \AA in the spectra dimension. The filter curve is the B_W bandpass convolved with the atmospheric transmission (blue). The 1σ error spectrum is overlaid (red).

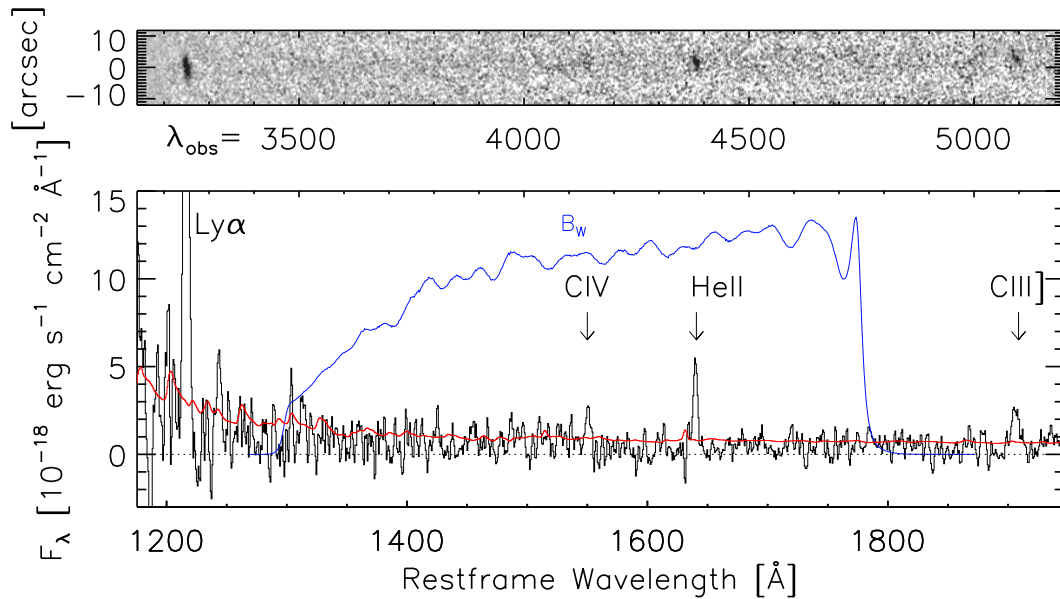


FIG. 3.— Night 2 (UT 2008 June 09) 2D and 1D spectra showing strong Ly α and He II emission, weak C III], and marginally-detectable C IV from a combined 1.5 hour exposure ($1.5 \times 5.0''$ aperture). The spectra are smoothed by $0.84''$ spatially and by 5.8 \AA in the spectral dimension. The filter curve is the B_W bandpass convolved with the atmospheric transmission (blue). The 1σ error spectrum is overlaid (red). When comparing to Figure 2, note that a 180° change in the slit position angle between the two nights caused a flip in the angle of the spectral trace across the detector.

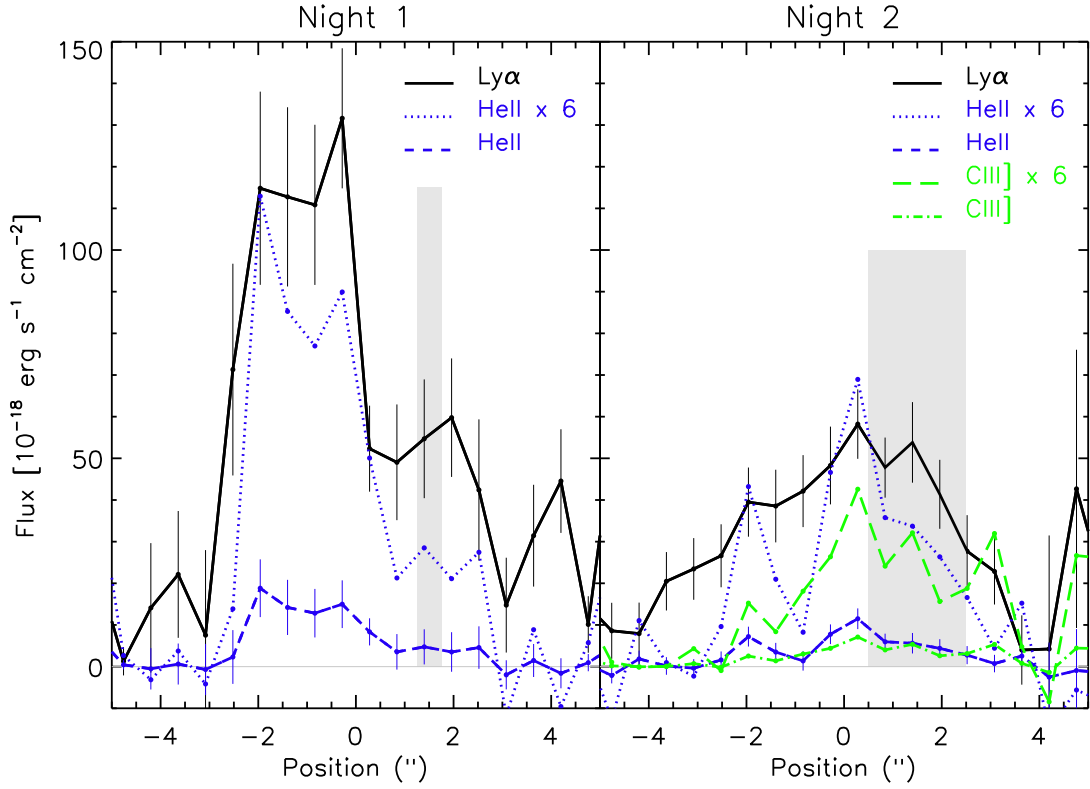


FIG. 4.— Ly α and He II spatial profiles with errors as a function of position along the slit from the Night 1 (UT 2008 June 08) and Night 2 (UT 2008 June 09). As C III] was not detected on Night 1, the C III] profile is shown for Night 2 only. He II and C III] profiles scaled by a factor of 6 are also overplotted to allow easier comparison with the Ly α profile. The He II region appears to be comparable in size to the Ly α region. The shaded area represents the approximate position of Source A, a source that was off-slit but that may have contaminated the Night 2 observations due to poor seeing and windy conditions. The discrepancy between the spatial profiles and the offset of the C III] spatial profile relative to the Ly α are both consistent with the hypothesis that the Night 2 spectrum is contaminated by light from Source A and that Source A may be the primary source of the metal line emission.

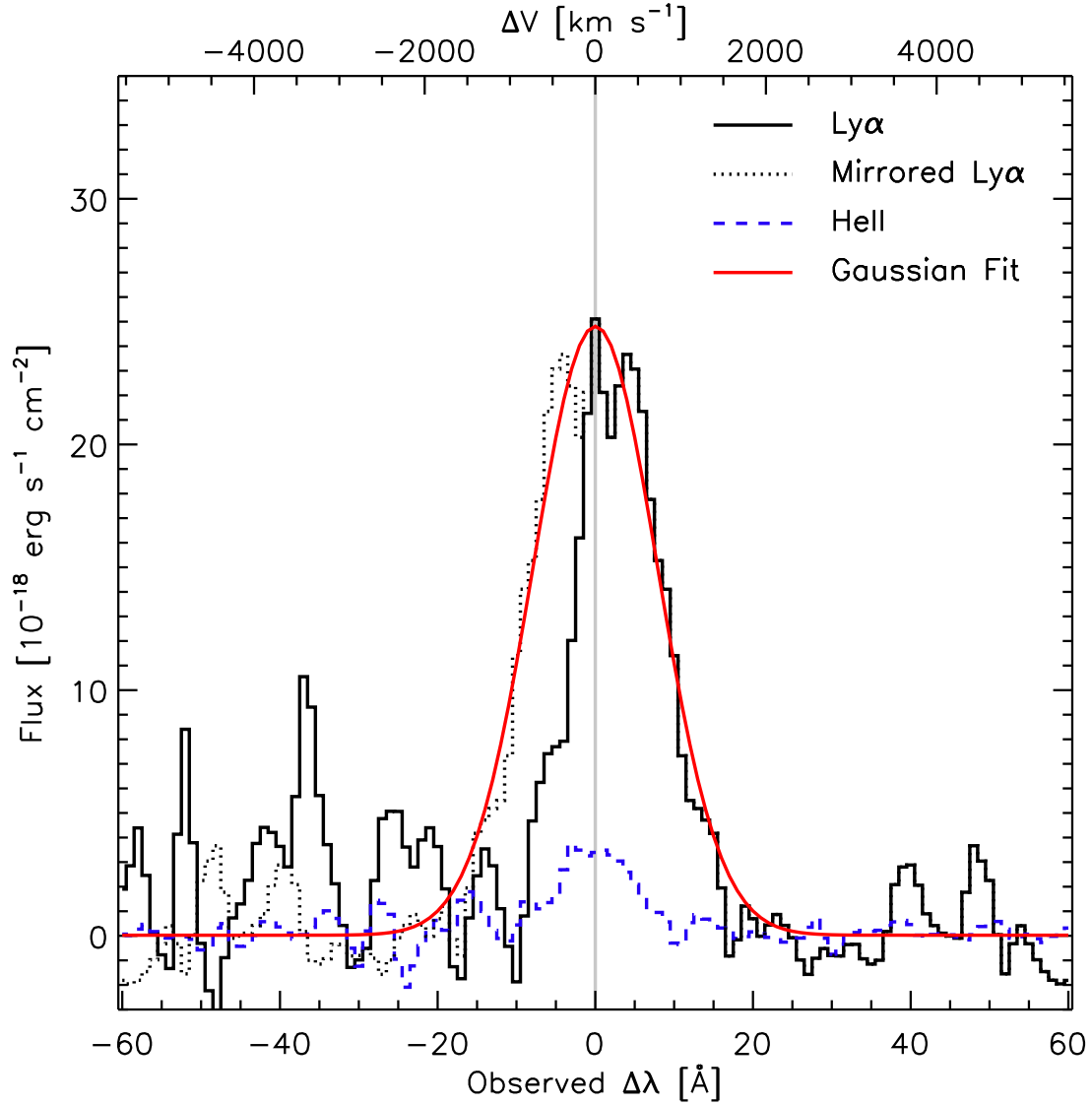


FIG. 5.— $\text{Ly}\alpha$ (black solid line) and He II (blue dashed line) line profiles as a function of observed wavelength centered on the systemic redshift of the system, as measured from the He II line. The observed $\text{Ly}\alpha$ is shown with the mirror image of the long-wavelength half of the line superimposed (black dotted line). A Gaussian fit (red solid line) indicates that the $\text{Ly}\alpha$ line may be absorbed by $\sim 41\%$. The corresponding velocity offsets for $\text{Ly}\alpha$ are given on the top axis.

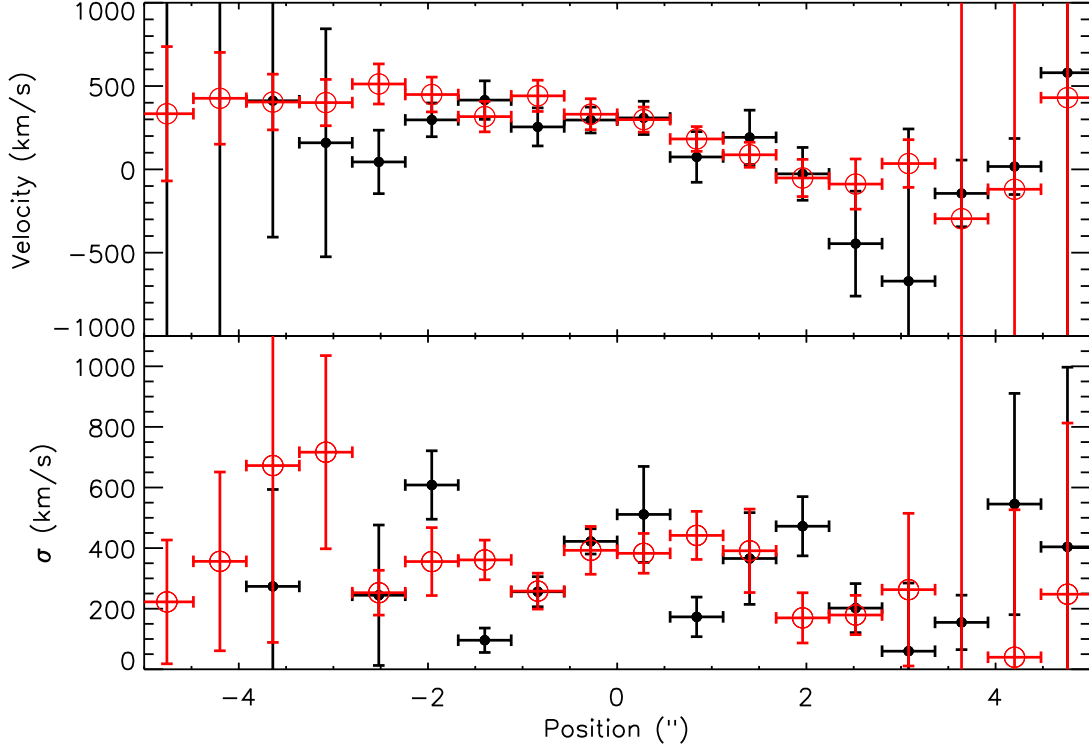


FIG. 6.— Velocity and velocity dispersion spatial profiles of the Ly α line for Night 1 (UT 2008 June 08; black filled circles) and Night 2 (UT 2008 June 09; red open circles) derived from spectra extractions taken in 2 pixel ($0.56''$) spatial bins and corrected for the instrumental resolution. The velocity zeropoint was set using the redshift calculated from the He II line centroid in the full $5.0''$ aperture extraction.

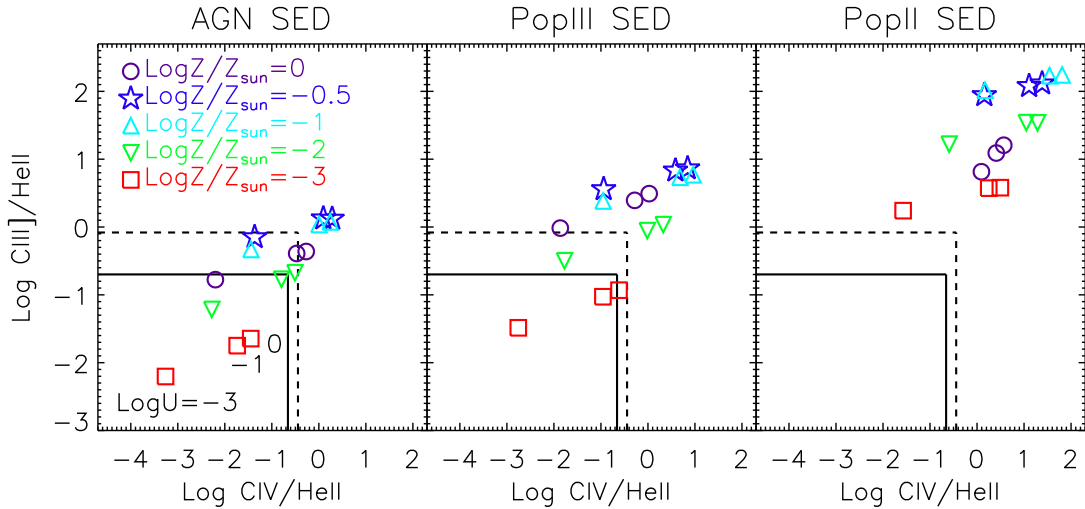


FIG. 7.— C III]/He II versus C IV]/He II line ratios for a grid of *CLOUDY* models over a range of SEDs, ionization parameters, and gas metallicities. The models represent a cloud of gas with $\text{Log}Z/Z_{\odot} = [-3, -2, -1, -0.5, 0]$ being ionized with an ionization parameter of $\text{Log}U = [-3, -1, 0]$ by one of three SEDs: an AGN SED (left), a Tumlinson et al. (2006) Population III galaxy model SED (middle; $Z=0$, 1 Myr burst, moderately top-heavy IMF discussed in the text), and a Starburst99 Population II galaxy model SED (right; $Z=0.001$, Salpeter IMF, 1 Myr burst; Leitherer et al. 1996). The 1σ limits on the line ratios of the nebulosity are shown for Night 1 (solid line) and Night 2 (dashed line).